Direct Measurement of Lateral Capillary Forces

Orlin D. Velev,† Nikolai D. Denkov,*,† Vesselin N. Paunov,†
Peter A. Kralchevsky,† and Kuniaki Nagayama‡

Laboratory of Thermodynamics and Physico-chemical Hydrodynamics, Faculty of Chemistry, University of Sofia, 1126 Sofia, Bulgaria, and Protein Array Project, ERATO, JRDC, 5-9-1 Tokodai, Tsukuba 300-26, Japan

Received May 21, 1993. In Final Form: August 31, 1993®

Precise and convenient force balance has been constructed for direct measurement of the lateral capillary forces between two vertical cylinders and between a cylinder and a wall. The experiments with both hydrophilic and hydrophobic capillaries of submillimeter diameter show that at large distances the capillary forces obey simple universal laws. A theoretical interpretation of this fact is proposed, which is based on a nonlinear superposition approximation for the shape of the liquid meniscus. At separations comparable with the capillary diameter and large slopes of the liquid surface, the nonlinear Laplace equation of capillarity should be solved numerically to describe the measured capillary forces. The obtained results have direct relation to the lateral capillary interactions between spherical particles floating on a single fluid interface or confined in a thin liquid layer.

1. Introduction

The lateral capillary interaction between colloid particles is a phenomenon pertinent to several important technological problems,[1,2] e.g. flotation of ores,[3] stability of Pickering emulsions,[4,5] formation of two-dimensional colloid crystals.[6-8] The theoretical calculation of the capillary interaction force and energy is a difficult problem because the meniscus shape should be determined by solving the Laplace equation of capillarity which represents a nonlinear partial differential equation. In the pioneering work of Nicolson[9] the capillary interaction energy between two bubbles attached to a liquid surface was calculated by assuming that the surface deformation is a mere superposition of the deformations created by the single bubbles (so called "linear superposition approximation"). Later several theoretical studies were published concerning the interaction between spheres floating on a single interface[10] (where the superposition approximation was used) or between two infinite horizontal cylinders laying on an interface.[10-12] In the latter case the general Laplace equation transforms into an ordinary differential equation.

In the last several years substantial progress was achieved by solving analytically the linearized Laplace equation (at small slopes of the meniscus around the particles) in bicylindrical coordinates.[13-17] General expressions were obtained for the capillary interaction energy and force between two vertical cylinders,[13,14] between two spheres,[14,17] between a sphere and a vertical wall,[15] and other configurations.[14,15] At large separations (much larger than the particle or cylinder diameter) the obtained expressions transform into the results stemming from the superposition approximation.[14,17] Two important conclusions of these studies, relevant to the present investigation, should be emphasized:

(i) The theoretical analysis shows that the capillary interaction between two spherical particles can be successfully approximated by the capillary interaction between two vertical cylinders, based on the three-phase contact lines of the particles[13,14]—see sections 4-6 in the work by Kralchevsky et al.[14] This makes the system of two vertical cylinders a convenient tool for performing direct measurements of the capillary forces and for comparison with the theoretical predictions.

(ii) Another result of the studies cited above is that the capillary force between two bodies obeys Newton's third law,[14-16] in spite of the fact that these forces stem from an indirect interaction due to the overlap of the menisci formed around the bodies. Hence, one can measure the force acting on one of the bodies and it must be certainly equal in magnitude to the capillary force acting on the other body.

It is worth mentioning that the lateral capillary forces between spherical particles partially immersed in a thin liquid layer[7,13,14] (we call them "immersion forces"[16,17]) can be many orders of magnitude greater than the forces between spheres similar in size, but *floating on a single interface*[9,10,17] (called "flotation forces"). The strong immersion capillary forces have been recognized to be among the main factors leading to the formation of two-dimensional colloid crystals from latex particles[6-8] or biocolloids[18-20] (protein molecules or viruses) on substrates.

* Author for correspondence.
† University of Sofia.
‡ Protein Array Project.
® Abstract published in *Advance ACS Abstracts*, October 15, 1993.

(1) Gerson, D. F.; Zaijc, J. E.; Ouchi, M. D. In *Chemistry for Energy*; Tomlinson, M., Ed.; ACS Symposium Series, American Chemical Society: Washington, DC, 1979; Vol. 90, p 77.
(2) Henry, J. D.; Prudich, M. E.; Vaidyanthan, K. P. *Sep. Purif. Methods* **1979**, *8*, 81.
(3) Schulze, H. J. *Physico-chemical Elementary Processes in Flotation*; Elsevier: Amsterdam, 1984.
(4) Levine, S.; Bowen, B. D. *Colloids Surf.* **1991**, *59*, 377.
(5) Denkov, N. D.; Kralchevsky, P. A.; Ivanov, I. B.; Wasan, D. T. *J. Colloid Interface Sci.* **1992**, *150*, 589.
(6) Denkov, N. D.; Velev, O. D.; Kralchevsky, P. A.; Ivanov, I. B.; Yoshimura, H.; Nagayama, K. *Nature (London)* **1993**, *361*, 26.
(7) Denkov, N. D.; Velev, O. D.; Kralchevsky, P. A.; Ivanov, I. B.; Yoshimura, H.; Nagayama, K. *Langmuir* **1992**, *8*, 3183.
(8) Dushkin, C. D.; Nagayama, K.; Miwa, T.; Kralchevsky, P. A. *Langmuir*, in press.
(9) Nicolson, M. M. *Proc Cambridge Philos. Soc.* **1971**, *45*, 288.
(10) Chan, D. Y. C.; Henry, J. D.; White, L. R. *J. Colloid Interface Sci.* **1981**, *79*, 410.
(11) Gifford, W. A.; Scriven, L. E. *Chem. Eng. Sci.* **1971**, *26*, 287.
(12) Fortes, M. A. *Can. J. Chem.* **1982**, *60*, 2889.
(13) Kralchevsky, P. A.; Paunov, V. N.; Ivanov, I. B.; Nagayama, K. *J. Colloid Interface Sci.* **1992**, *151*, 79.
(14) Kralchevsky, P. A.; Paunov, V. N.; Denkov, N. D.; Ivanov, I. B.; Nagayama, K. *J. Colloid Interface Sci.* **1993**, *155*, 420.
(15) Paunov, V. N.; Kralchevsky, P. A.; Denkov, N. D.; Ivanov, I. B.; Nagayama, K. *Colloids Surf.* **1992**, *67*, 119.
(16) Kralchevsky, P. A.; Nagayama, K. *Langmuir*, in press.
(17) Paunov, V. N.; Kralchevsky, P. A.; Denkov, N. D.; Nagayama, K. *J. Colloid Interface Sci.* **1993**, *157*, 100.

0743-7463/93/2409-3702$04.00/0

We are aware of only one study, ref 21, where the lateral capillary forces between millimeter-sized polystyrene spheres were measured. Unfortunately, in this study no information is presented about the three most important parameters of the investigated system: interfacial tension, three-phase contact angle, and radii of the three-phase contact lines. Therefore, the results from the work of Camoin et al.[21] cannot be used for direct comparison with the theory.

Our aim in this study is to measure directly the capillary force between two vertical cylinders as well as between a vertical cylinder and a wall, at well-defined conditions. For interpretation of the experimental results, theoretical expressions are derived and the range of their validity is established. We can say in advance that at large separations the dimensionless interaction force (and energy) obeys an universal law independently on whether the slope of the meniscus around the capillaries and the wall is large or small. A theoretical explanation of this experimental fact is proposed, which resembles the method developed by Verwey and Overbeek[22] for calculating the electrostatic interaction between strongly charged surfaces in electrolyte solutions (the so-called "nonlinear superposition approximation").[23,24] At small separations, however, the interaction is much stronger than the one predicted by the superposition theories.

The article is organized as follows: section 2 presents the theoretical expressions for the lateral capillary forces; section 3 describes the materials used; section 4 presents the capillary force balance and the procedures of calibration and measuring; section 5 discusses the experimental results; section 6 summarizes the conclusions; the nonlinear superposition approximation is applied to calculate the capillary force and energy in the Appendix.

2. Theoretical Expressions for the Capillary Forces between Two Vertical Cylinders and between a Cylinder and a Wall

Before the experimental results are presented, it is instructive to consider briefly the theoretical expressions for the lateral capillary forces. We restrict ourselves to the case of two vertical cylinders of submillimeter radii ($qr_k \ll 1, k = 1, 2$, see below) and to the case of interaction between a vertical submillimeter cylinder and a vertical wall.

Let us denote by q^{-1} the so-called capillary length

$$q = \left(\frac{\Delta\rho g}{\gamma}\right)^{1/2} \tag{2.1}$$

where $\Delta\rho$ is the difference between the mass densities of the two fluid phases, g is the gravity acceleration, and γ is the surface tension.

We start with the case of two vertical cylinders. The ability of the cylinders to deform the fluid interface can be characterized by their "capillary charges"[16,17]

$$Q_k = r_k \sin\psi_k; \qquad k = 1, 2 \tag{2.2}$$

with r_k ($k = 1, 2$) being the radius of cylinder 1 or 2 and

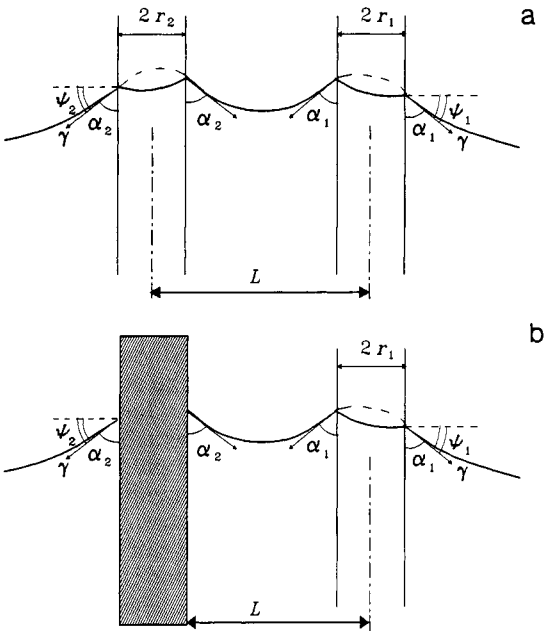

Figure 1. Geometry of the systems under consideration: (a) two vertical cylinders; (b) a vertical cylinder and a wall (plate). α_k ($k = 1, 2$) denotes the three-phase contact angles.

ψ_k being the meniscus slope angles at the three-phase contact lines; see Figure 1a. The latter is connected with the corresponding three-phase contact angle α_k measured through the lower phase (Figure 1a):

$$\psi_k = \frac{\pi}{2} - \alpha_k, \qquad k = 1, 2 \tag{2.3}$$

If the contact angles α_k are close to $\pi/2$ (that is if $\sin^2\psi_k \ll 1, k = 1, 2$), the meniscus slope is small over the entire fluid interface. Then one can use the linear superposition approximation[9,10] for the shape of the meniscus if the distance between the axes of the cylinders, L, is much larger than their radii ($r_k/L \ll 1, k = 1, 2$). The capillary force can be calculated in this case and the result reads[10,17]

$$F(L) = 2\pi q\gamma Q_1 Q_2 K_1(qL) \tag{2.4}$$

$$r_k/L \ll 1$$

where $K_1(x)$ is the modified Bessel function of first order. This expression has simple asymptotes at large and small separations (in comparison with the capillary length q^{-1})

$$F(L) \approx 2\pi\gamma Q_1 Q_2 \frac{1}{L} \tag{2.5}$$

$$qL \ll 1$$

and

$$F(L) \approx \pi\gamma Q_1 Q_2 \left(\frac{2\pi q}{L}\right)^{1/2} e^{-qL} \tag{2.6}$$

$$qL \geq 2$$

The latter expression shows that at large distances F decays roughly exponentially (as found experimentally by Camoin et al.[21]) with a decay length equal to q^{-1}. That is why the capillary length is often used to characterize the range of capillary interactions.

Kralchevsky et al.[13-17] solved analytically the linearized Laplace equation in bicylindrical coordinates and thus avoided the necessity to involve the superposition approximation. Hence, their results are applicable even at very small separations provided that the meniscus slope

(18) Yoshimura, H.; Endo, S.; Matsumoto, M.; Nagayama, K.; Kagawa, Y. *J. Biochem.* **1989**, *106*, 958.
(19) Yoshimura, H.; Matsumoto, M.; Endo, S.; Nagayama, K. *Ultramicroscopy* **1990**, *32*, 265.
(20) Nagayama, K. *Nanobiology* **1992**, *1*, 25.
(21) Camoin, C.; Roussell, J. F.; Faure, R.; Blanc, R. *Europhys. Lett.* **1987**, *3*, 449.
(22) Verwey, E. J. W.; Overbeek, J. Th. G. *Theory of the Stability of Lyophobic Colloids*; Elsevier: Amsterdam, 1948.
(23) Russel, W. B.; Saville, D. A.; Schowalter, W. R. *Colloidal Dispersions*; Cambridge University Press: Cambridge, 1989.
(24) Derjaguin, B. V.; Churaev, N. V.; Muller, V. M. *Surf. Forces*; Consultants Bureau, Plenum Press: New York, 1987.

is small ($\sin^2 \psi_k \ll 1$) and the cylinder radius is much smaller than the capillary length ($qr_k)^2 \ll 1$). The numerical calculations showed that at separations much larger than the cylinder radius ($r_k/L \ll 1$) the superposition approximation yields correct results for the capillary force.[14,17] However, at small separations ($L \sim r_1 + r_2$) the superposition approximation strongly underestimates the capillary force.[17]

All the theoretical expressions discussed above were derived under the assumption that the meniscus slope is small everywhere, including the regions in vicinity of the cylinder surfaces. However, in the experiments presented below the contact angle of the used glass capillaries is close to zero and the theory should be extended to cover the case of large meniscus slope. Our measurements showed (see section 5) that eq 2.4 remains valid at large separations ($r_k/L \ll 1$) even for very small contact angles ($\alpha_k \approx 0; \psi_k \approx \pi/2; k = 1, 2$) when the meniscus slope is very large in a vicinity of the cylinder surfaces. In the Appendix we show that this experimental fact can be explained by assuming that the surface deformation is a superposition of the deformations created by two single cylinders, at least at sufficiently large distances from the cylinders where the meniscus slope is small. A similar assumption has been used in colloid science for many years[22,24] to explain the electrostatic interaction between strongly charged surfaces or spherical particles and is known as "the nonlinear superposition approximation".[23] Hence, eq 2.4 has a wider range of validity than thought previously.

For the interaction between a vertical cylinder and a wall in the framework of the *linear* superposition approximation (small meniscus slope everywhere), we derive (see the Appendix)

$$F(L) \approx 2\pi\gamma Q_1 \tan \psi_2 e^{-qL} \tag{2.7}$$

L in this case denotes the distance between the axis of the cylinder and the wall surface and ψ_2 characterizes the meniscus slope at the wall; see Figure 1b. Then we apply the *nonlinear* superposition approximation which leads to the expression (see the Appendix)

$$F(L) \approx 2\pi\gamma D Q_1 e^{-qL} \tag{2.8}$$

$$qL \gg 1$$

where

$$D = 4\left(\tan\frac{\psi_2}{4}\right)\exp\left(-4\sin^2\frac{\psi_2}{4}\right) \tag{2.9}$$

Equation 2.8 reduces to eq 2.7 if $\sin^2 \psi_2 \ll 1$. Both expressions, eqs 2.7 and 2.8, are not applicable if $\sin \psi_2 \leq qr_1 \sin \psi_1 \ll 1$ (i.e. if α_2 is very close to 90°); see eq A.29 and the respective discussion in the Appendix. It turns out (section 5 below) that eq 2.8 describes very well the experimental results at large separations ($qL > 1$). However, at small separations ($qL \leq 1$) and large meniscus slope ($\psi_k \approx 90°$) the experiment shows that eq 2.8 underestimates the magnitude of the capillary force, as should be expected (for details see below).

3. Materials

The water for the experiments and for preparing the solutions was extracted from a Milli-Q Organex system, Millipore. In some of the experiments surfactant solutions of sodium dodecyl sulfate (SDS) were used. The surfactant was a Sigma product for laboratory use and was applied without additional purification. All of the solutions were prepared shortly before the experiments from a recently obtained batch quantity of SDS. The cylindrical capillaries for the experiments were produced from glass tubes for laboratory purposes, product of Jena, Germany. The surface of the capillaries was initially precleaned by dipping them for 15 min in 4 wt % of hydrofluoric acid. In some experiments a hydrophilic glass plate was used. It was prepared by sandblasting the surface of a microscope cover glass (24 × 32 × 0.17 mm; Ilmglas, Germany). Before each of the experimental runs the capillaries and the plate were cleaned by immersion into hot chromic acid and leaving them inside for not less than 24 h, followed by abundant rinsing with water. Hot chromic acid was used also for cleaning the cuvette and the instrumental glassware. The capillary diameters were measured by an optical microscope.

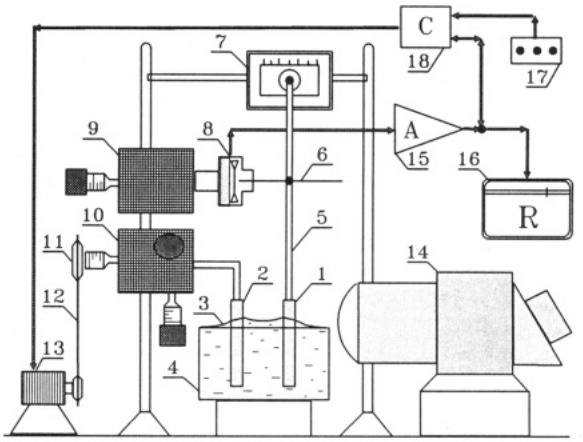

Figure 2. Scheme of the setup for capillary force measurements: (1 and 2) cylinders between which the force is measured (not in scale); (3) surface of the liquid phase with curved menisci around the capillaries; (4) cuvette holding the liquid phase; (5) glass lever; (6) glass probe; (7) fiber galvanometer; (8) piezoresistive sensor; (9) sensor positioner; (10) $xyz\varphi$ positioner; (11 and 12) belt and pulley drive; (13) motor; (14) long focus microscope; (15) compensated dc amplifier; (16) recorder; (17) remote control console; (18) motor controller. The diameters of the depicted capillaries are strongly exaggerated compared to the size of the vessel.

In some measurements we used hydrophobized glass capillaries and plates. The hydrophobization was accomplished by immersion of the precleaned glass surface into 10 vol % solution of dimethylchlorsilane in toluene for 5 h, followed by rinsing with pure methanol and water.

The surface tension of water and of surfactant solutions was measured by the Wilhelmi-plate method.

4. Balance for Capillary Force Measurements

4.1. Experimental Setup. A special type of balance was designed and used for measurement of the capillary forces between bodies protruding from the liquid surface. The schematics of the balance are presented in Figure 2. The basic scheme of the setup was borrowed from a similar device aimed at measuring the viscosity of the liquid in thin layers between solid plates.[25,26]

Two vertical cylinders or alternative bodies denoted by (1) and (2) in Figure 2, are protruding from the surface of the liquid (3). Menisci are formed around the cylinders, which leads to the appearance of a lateral capillary force between them. One of the cylinders (denoted by (1) in Figure 2) is connected to the balance which measures the horizontal component of the force exerted on it. The other cylinder (2) can be moved during the experiments in order to change the distance between the bodies. Two thin glass capillaries or a capillary and a plate (see Figure 1) were

(25) Velev, O. D. M.Sc. Thesis, University of Sofia, Faculty of Chemistry, 1989.

(26) Nikolov, A. D.; Velev, O. D.; Shetty, C. S. Unpublished results.

used in our measurements. The distance between the cylinder or plate and the wall of the glass container with solution (4) is sufficiently large in order to avoid any disturbance of the measured force.

A precise piezoresistive sensor (8), originally designed as a sensitive pressure transducer (163PC01D, Microswitch, Inc., USA), is used to convert the force to an electric signal. The force is applied to the sensor membrane through the glass lever (5) and the probe (6). In order to assure high mechanical sensitivity, the delicate lever is suspended at the arrow of a fiber galvanometer (7). The alignment of the sensor against the probe is accomplished through the sensor positioner (9). The electrical response of the sensor (proportional to the force exerted on cylinder 1) is processed through a compensated dc amplifier (15) and is recorded by a potentiometric recorder (16). The rigidity of the sensor membrane and the lever provides the practical immobility of cylinder 1 during the experiments.

The parallel alignment of the cylinders and the distance between them is carried out through a positioner (10) with four degrees of freedom. The x-direction micrometric screw of the positioner is driven by a pulley (11) and belt (12) attached to a synchronous reversible motor (13). The motor speed and direction are regulated by a controller (18) through the remove control console (17). The distance between the cylinders is measured by using a long focus optical microscope (14). Special attention is paid to avoid vibrations and drift of the base line of the measuring system.

It was shown (see the next subsection) that the balance has a linear response to an applied force.

4.2. Calibration. In order to ensure the reading of the net force and to check the system linearity and performance, a procedure for calibration of the balance was developed. A second magnetoelectric galvanometer system with a glass lever extension attached to the galvanometer arrow was used for that purpose. The magnetoelectric system is mounted on a movable stand and electrically connected to a regulated dc current supply with digital current meter. With a change of the current into the magnetoelectric system, different forces are applied to the thin glass lever. During the calibration this lever is pressed against cylinder 1 (see Figure 2) at the level of the water meniscus. The response of the balance toward these different applied forces is recorded. The same forces are later measured directly by pressing the lever of the calibration system against a precise analytical balance (Sartorius Research 160P) and applying the corresponding electric currents.

The calibration procedure was carried out after each of the experimental runs and the results were fairly reproducible. The usable sensitivity of the balance for the capillary force measurements is estimated as better than $\pm 3 \times 10^{-7}$ N. The linearity within the measured range of forces is better than ±1%. The precision in measuring the distance between the cylinders by means of the microscope is ±5 μm.

4.3. Procedure of Measurements. Before an experimental run is carried out, the cylinders are adjusted to parallel, the aqueous phase is poured inside the cuvette, and its surface is additionally cleaned from impurities by suction of liquid with an appropriate pipet. In most of the experiments cylinder 2 is slowly driven apart or brought closer to cylinder 1 at a constant rate of about 0.5 μm/s. Thus the force *vs* time output from the recorder can be directly recalculated as force *vs* distance curve. In each measurement, the baseline (zero force) was checked before and after the run by separating the cylinders at a long distance apart. The obtained curves from the independent

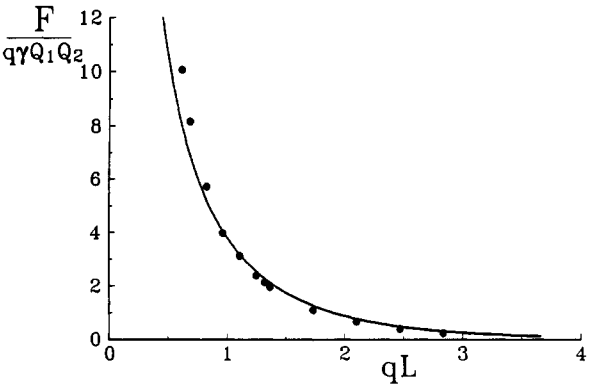

Figure 3. Dimensionless capillary force between two hydrophilic glass cylinders as a function of qL. The parameters are $\alpha_1 = \alpha_2 = 0$, $r_1 = 370 \pm 5$ μm, $r_2 = 315 \pm 5$ μm, and $\gamma = 72.4 \pm 0.5$ mN/m. The solid curve is calculated from eq 2.4.

measurements show a good reproducibility; the data reported in section 5 are averaged over three or more experimental curves.

In order to ensure that the measured force does not include contributions from the hydrodynamic resistance of the moving cylinders, some experiments were carried out in a stepwise separation manner: consecutively fixing the distance between the cylinders and leaving the system immobile for more than 60 s. The data obtained in this manner coincide with the data for the slowly moving cylinders. Therefore no detectable hydrodynamic contribution to the measured force is assumed. In the experiments with plate and cylinder only stepwise measurements were carried out.

5. Experimental Results and Discussion

Figure 3 presents the dimensionless capillary force $F/(q\gamma Q_1 Q_2)$ between two hydrophilic glass cylinders as a function of the dimensionless distance qL. In this case $\alpha_1 = \alpha_2 \approx 0$, $r_1 = Q_1 = 370 \pm 5$ μm, and $r_2 = Q_2 = 315 \pm 5$ μm. The liquid phase is pure water with surface tension $\gamma = 72.4 \pm 0.5$ mN/m, which corresponds to a capillary length $q^{-1} = 2.72$ mm. The experimental data are averaged over three independent runs and are presented by the solid circles. The reproducibility and accuracy of the data are indicated by the size of the circles. The force is attractive (positive in our convention) and slowly decays with the interparticle distance. The magnitude of the force is $F = 1.25 \times 10^{-5}$ N at $qL \approx 1$. The solid curve in Figure 3 presents the result predicted by eq 2.4. It is seen that at large distances ($qL \geq 1$) the experimental data are very well represented by the theoretical expression. At small separations (down to $qL \approx 0.5$) eq 2.4 underestimates the force. We were not able to measure the force at distances $qL < 0.5$ under these conditions because its magnitude steeply increases and below some critical separation the two capillaries stick to each other.

One should note that in the case of glass cylinders in pure water, the hysteresis of the three-phase contact angle is appreciable and the force between the cylinders depends on whether they are approaching or receding. The force between approaching cylinders (even very well cleaned) is typically 10–15% lower in magnitude and badly reproducible. The force between receding cylinders (shown in Figure 3) is very well reproducible (within 1–2%) and stronger. This observation can be explained by considering the movement of the three-phase contact lines along the cylinder surfaces. When the cylinders are separating from each other, the contact lines are moving down along the cylinders (see Figure 4). Hence, we have receding meniscus with a contact angle α very close the equilibrium angle 0.

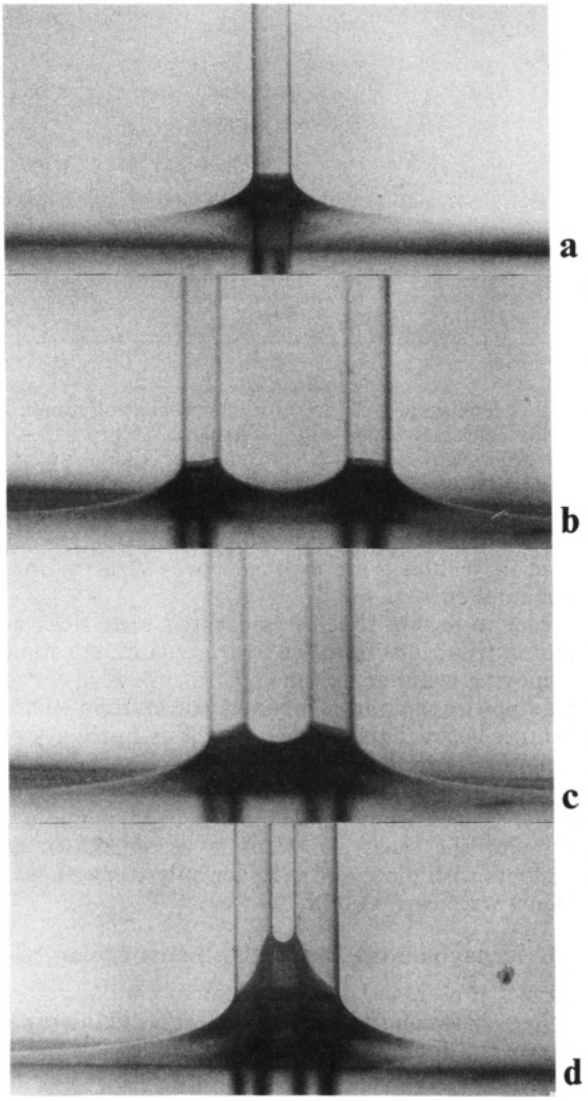

Figure 4. Photographs of the meniscus and of the three-phase contact lines at different separations, L, between two hydrophilic capillaries: (a) meniscus around a single capillary, (b) $L = 2.775$ mm, (c) $L = 1.760$ mm, (d) $L = 1.055$ mm. The liquid phase is 8×10^{-2} M SDS solution with $\gamma = 36.8 \pm 0.5$ mN/m. The other parameters are $\alpha_1 = \alpha_2 = 0$, $r_1 = 370 \pm 5$ μm, $r_2 = 315 \pm 5$ μm.

If the cylinders are approaching each other, the capillary rise corresponds to advancing meniscus. We found out experimentally that the advancing contact angle is slightly larger than the equilibrium angle and it is not very well reproducible. That is why in Figure 3 we present only the results from the measurements with separating cylinders.

In Figure 5 the results for the same cylinders partially immersed in 8×10^{-2} M sodium dodecyl sulfate (SDS) are presented. Since the surface tension $\gamma = 36.8 \pm 0.5$ mN/m is lower in this case, the calculated capillary length (see eq 2.1) is shorter: $q^{-1} = 1.92$ mm. The other parameters of the system are the same. The solid curve is calculated by means of eq 2.4. It is seen that for large separations the experimental points tend again to the theoretical prediction. At small separations the superposition approximation underestimates the capillary force. One should notice that although the actual radii of the cylinders are the same, the dimensionless radii qr_k ($k = 1, 2$) are larger than those in the former experiment with pure water. Probably this is the reason why the deviations from the theoretical expressions (i.e. the nonlinear effects) at the same dimensionless separation, qL, are larger in Figure 5 compared to Figure 3. The hysteresis of the three-phase contact angle (and of the capillary force) was negligible in

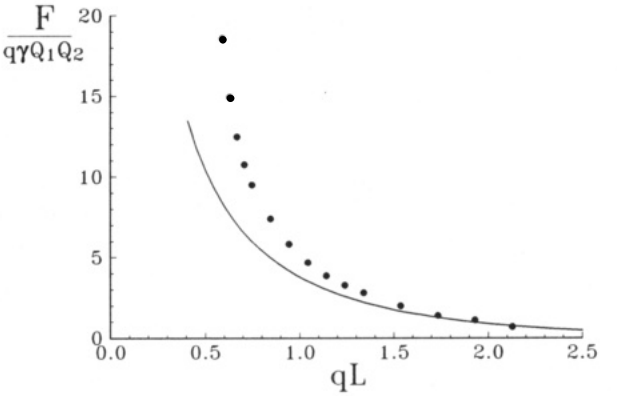

Figure 5. Measured capillary force between two glass capillaries in 8×10^{-2} M SDS solution. The parameters are the same as in Figure 4. The solid curve is calculated from eq 2.4.

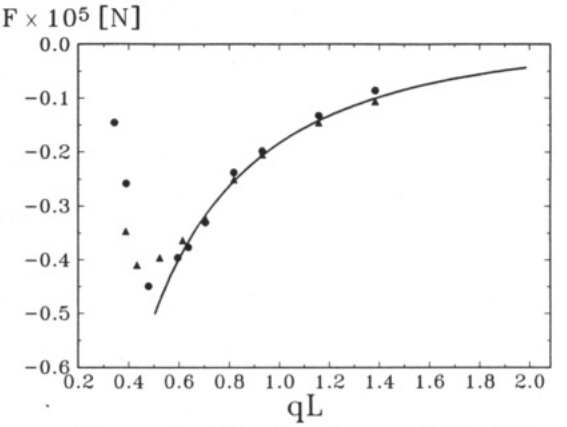

Figure 6. Measured capillary force between hydrophilic ($\alpha_1 = 0$, $r_1 = 370 \pm 5$ μm) and hydrophobic ($\alpha_2 = 99°$, $r_2 = 315 \pm 5$ μm) capillaries in pure water ($\gamma = 72.4 \pm 0.5$ mN/m). The results from two independent runs are shown with circles and triangles. The solid curve is calculated from eq 2.4.

this case. The forces between approaching and separating cylinders are practically the same for this system and extremely well reproducible (within 1–2%). Obviously, this is due to the fact that the glass surface is very well wetted by the SDS solutions.

Figure 6 shows the capillary force between a hydrophilic ($\alpha_1 \approx 0$) and a hydrophobic ($\alpha_2 > 90$) cylinder immersed in pure water. As predicted by eqs 2.2–2.4 the cylinders repel each other at large separations ($Q_1Q_2 < 0$; the force is negative). The radii of the cylinders are $r_1 = 370 \pm 5$ μm (hydrophilic capillary) and $r_2 = 315 \pm 5$ μm (hydrophobic capillary). Since α_2 is an unknown parameter, we determined it from the data at large separations. Assuming that eq 2.4 is valid at $qL \geq 0.6$, we calculated $\alpha_2 = 99 \pm 0.5°$. Surprisingly, at small separations ($qL < 1$) the magnitude of the capillary force decreases and probably at very small separations (not achieved in our experiments) it changes from repulsive to attractive. The microscope observations showed that at small separations the shape of the three-phase contact line at the hydrophobic capillary changed; compare parts a and b of Figure 7. At large distances ($L/(r_1 + r_2) \geq 2$) the contact line around the hydrophobic cylinder (the left one in Figure 7a) is entirely below the liquid surface level and is not visible in the figure. At smaller distances one observes that the contact line on the hydrophobic cylinder rises above the liquid level in the portion closer to the hydrophilic cylinder. This is a nonlinear effect, which can be rigorously described only by solving the nonlinear Laplace equation of capillarity.

The experimental results for the capillary force between a completely wettable capillary and a plate ($\alpha_1 = \alpha_2 = 0$)

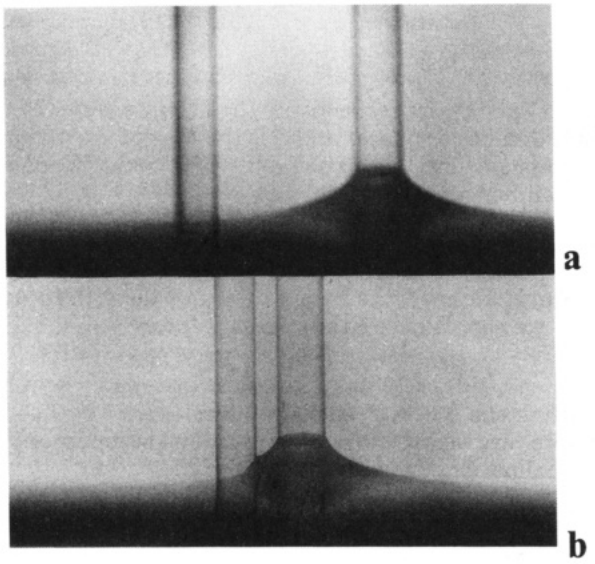

Figure 7. Photographs of the meniscus around hydrophilic and hydrophobic capillaries at separations L = 2.830 mm (a) and at L = 1.025 mm (b). The other parameters are the same as in Figure 6.

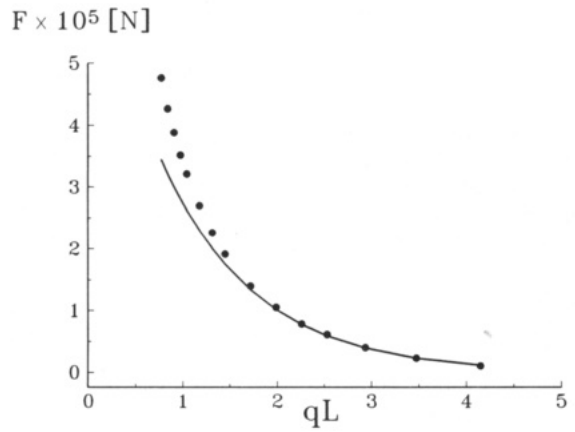

Figure 8. Measured capillary force between a hydrophilic capillary (α_1 = 0, r_1 = 370 μm) and a plate (α_2 = 0). The solid curve is calculated from eq 2.8.

are plotted in Figure 8. The bodies are protruding from a 2.5 × 10^{-2} M SDS solution. The radius of the capillary is r_1 = 370 ± 5 μm. The capillary force is much stronger in this case and can be detected at long distances away from the wall. One sees that at separations $qL > 1.5$ the experimental points agree very well with eq 2.8, (the solid line): q^{-1} = 1.88 mm, γ = 35 ± 0.5 mN/m. At smaller separations the superposition approximation again underestimates the force.

In Figure 9 the measured force between a hydrophobized glass plate ($\alpha_2 > \pi/2$) and a hydrophilic capillary (α_1 = 0, r_1 = 370 μm) is presented. The force is repulsive and increases in magnitude at decreasing separations. By assuming that eq 2.8 is applicable at $qL > 1.5$ and considering α_2 as an adjustable parameter, we calculated D = −0.49 ± 2% and then eqs 2.3 and 2.9 yield α_2 = 120 ± 3°. Again at small separations one observes deviation of the experimental points from the theoretical values predicted by eq 2.8 (the solid curve).

6. Conclusions

In this study we present experimental measurements of the lateral capillary interaction between two vertical cylinders and between a vertical cylinder and a wall. The specially designed force balance (Figure 2) allows direct measurement of both attractive and repulsive forces. It

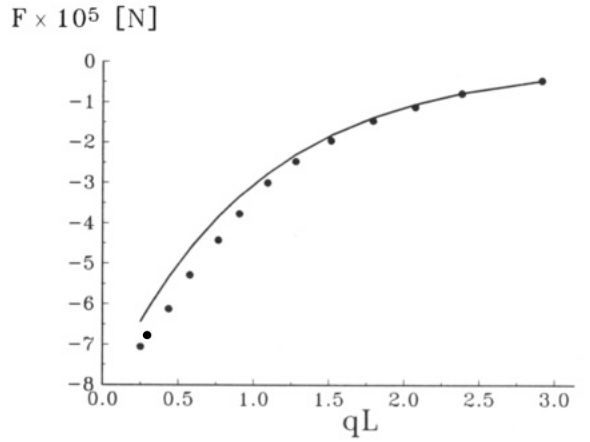

Figure 9. Measured capillary force between a hydrophilic capillary (α_1 = 0, r_1 = 370 μm) and a hydrophobic plate (α_2 = 120°). The solid curve is calculated from eq 2.8.

can be applied without substantial transformation to other systems of interest, e.g. interaction between spheres or interaction between bodies partially immersed in a thin liquid film.

The experimental data show that at large separations the capillary force is well described by simple formulas; see eqs 2.4 and 2.8 and Figures 3, 6, 8, and 9. The nonlinear superposition approximation is involved to calculate theoretically the capillary force and to explain this experimental fact; see the Appendix. At small separations the expressions derived on the basis of the superposition approximations do not describe quantitatively the capillary force, as it could be expected. Moreover, in some particular cases the experiment shows that the interaction force can go through a minimum (see Figure 6) and eventually can change its sign. The theoretical interpretation of the data at small separations and large meniscus slope needs a numerical integration of the nonlinear Laplace equation of capillarity, which is a matter of future development.

Acknowledgment. This work was supported by the Research and Development Corporation of Japan (JRDC) under the program Exploratory Research for Advanced Technology (ERATO). Useful discussions with Professor I. B. Ivanov are gratefully acknowledged.

Appendix. Nonlinear Superposition Approximation and Capillary Forces

This Appendix is devoted to the derivation of eqs 2.4 and 2.8.

1. Capillary Meniscus Interaction between Two Vertical Cylinders. We consider the interaction between two vertical cylinders; see Figures 1a and 10. The coordinate plane xy is chosen to coincide with the flat fluid interface far from the cylinders. The x-axis crosses the axes of the two cylinders. The shape of the meniscus is given by the function

$$z = \zeta(x,y) \qquad \text{(A.1)}$$

Three types of forces are exerted on each of the cylinders: the hydrostatic pressure, the interfacial tension, and an outer force which keeps the cylinders separated at a distance L. It is the horizontal projection of these forces that will be considered below. The sum of the forces due to the hydrostatic pressure and the interfacial tension gives the capillary force which is exactly counterbalanced by the outer force. In the previous considerations[14-16] the capillary force was calculated by direct integration of the pressure over the cylinder surface and of the interfacial tension acting on the three-phase contact line. However,

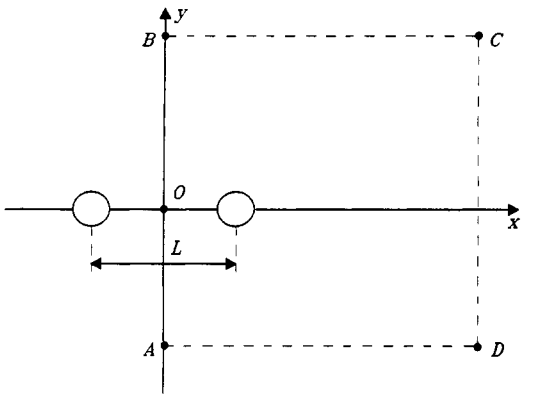

Figure 10. Integration contour for calculating the capillary force between two cylinders.

the capillary force can be calculated in an alternative way by integrating the pressure and interfacial tension over an arbitrary volume of the system which includes one of the cylinders. Since the system is considered to be in equilibrium, such an integral over a fluid volume must be counterbalanced by the outer force. Hence, the integral is exactly equal to the capillary force acting on the cylinder. In fact, this is an application of the principle of Stevin in the hydrostatics, proposed long ago. This method enables one to calculate the capillary force even when the meniscus slope close to the cylinders is large and the Laplace equation cannot be linearized. Nevertheless, when L is large enough, there is a region with small slope in the middle between the two cylinders. The latter fact is utilized in the method of the nonlinear superposition approximation described below.

Let us choose the contour of integration to be a square with a side laying on the Oy-axis; see Figure 10. The size of the square is much larger than q^{-1}, i.e. the portions, BC, CD, and DA are in the regions where the interface is practically flat ($\zeta = 0$). We have $\zeta \neq 0$ only along the segment AB where the profile of the fluid interface is given by the function

$$\zeta_0(y) \equiv \zeta(x=0,y) \tag{A.2}$$

The x-component of the net force due to the interfacial tension acting on the sides of the square is given by the expression

$$F^{(\gamma)} = \mathbf{e}_x \cdot \int_{ABCD} \gamma \, dl \approx \gamma \int_0^\infty \left[\left(\frac{d\zeta_0}{dy}\right)^2 - \left(\frac{\partial \zeta}{\partial x}\right)^2_{x=0} \right] dy \tag{A.3}$$

where $\mathbf{e}_x$ is unit vector, γ is the vector of the interfacial tension and the integration is performed along the contour ABCD shown in Figure 10. The integrals along the segments BC and DA cancel each other owing to the symmetry of the system. We have used also the fact that because of the small slope of the meniscus along the contour of integration one can write

$$\mathbf{e}_x \cdot \gamma = \gamma \cos \psi = \frac{\gamma}{(1 + \tan^2 \psi)^{1/2}} \approx \gamma \left[1 - \frac{1}{2} \left(\frac{\partial \zeta}{\partial x}\right)^2 \right]$$

$$dl = \left(1 + \left(\frac{d\zeta_0}{dy}\right)^2\right)^{1/2} dy \approx \left[1 + \frac{1}{2}\left(\frac{d\zeta_0}{dy}\right)^2\right] dy \tag{A.4}$$

where ψ is the meniscus slope angle. The x-component of the force due to the hydrostatic pressure is given by the integral

$$F^{(p)} = -\mathbf{e}_x \cdot \int_S P \, d\mathbf{s} \tag{A.5}$$

where

$$P = p_0 - \rho_1 g z \qquad \text{at } z < \zeta_0(y) \tag{A.6}$$

$$P = p_0 - \rho_2 g z \qquad \text{at } z > \zeta_0(y)$$

Here ρ_1 and ρ_2 are respectively the mass densities of the lower and upper phases and S is the area of the plane zy encompassed by the y-axis and the $\zeta_0(y)$ curve. Equation A.5 can be transformed to read

$$F^{(p)} = \Delta\rho g \int_0^\infty \zeta_0^2(y) \, dy \tag{A.7}$$

Hence, if we know the meniscus shape along the y axis, $\zeta_0(y)$, we can calculate the capillary force

$$F = F^{(\gamma)} + F^{(p)} \tag{A.8}$$

by using eqs A.3, A.7, and A.8.

Here we make use of the nonlinear superposition approximation, i.e. we assume that

$$\zeta_0(y) = \zeta_1(y) + \zeta_2(y) \tag{A.9}$$

where $\zeta_k(y)$ is the deformation created by the single cylinder k ($k = 1, 2$) at the given point. As shown by Derjaguin,[27] the deformation of the liquid surface far away from a single cylinder is given by

$$\zeta_k(r) = Q_k K_0(qR_k) \tag{A.10}$$

$$k = 1, 2, \quad qQ_k \ll 1$$

where R_k is the distance from the point, r, in the plane xy to the respective cylinder axis, Q_k is given by eq 2.2, and K_0 is a modified Bessel function. If the segment AB is situated at an equal distance, s, from the two cylinder axes, then $R_k^2 = y^2 + s^2$ and eq A.9 can be written as

$$\zeta_0(y) = (Q_1 + Q_2) K_0(q(y^2 + s^2)^{1/2}) \tag{A.11}$$

$$s \equiv L/2$$

Then one can calculate

$$F^{(\gamma)} = \gamma q^2 \int_0^\infty \frac{K_1^2(q(y^2 + s^2)^{1/2})}{y^2 + s^2} [(Q_1 + Q_2)^2 y^2 - (Q_1 - Q_2)^2 s^2] \, dy \tag{A.12}$$

$$F^{(p)} = \gamma q^2 \int_0^\infty (Q_1 + Q_2)^2 K_0^2(q(y^2 + s^2)^{1/2}) \, dy \tag{A.13}$$

The numerical integration of eqs A.12 and A.13 along with eq A.8 shows that the sum of the two integrals for $F^{(\gamma)}$ and $F^{(p)}$ is just equal to the expression

$$F = 2\pi q \gamma Q_1 Q_2 K_1(qL) \tag{A.14}$$

(We have not found a way to prove analytically that the sum of the integrals A.12 and A.13 is equivalent to expression A.14.)

2. Interaction between a Vertical Cylinder and a Wall. The shape $z(x)$ of the liquid meniscus in the vicinity of a single vertical wall is given by the parametric equations[28]

$$qz = 2 \sin \frac{\psi}{2} \tag{A.15}$$

$$qx = -2 \cos \frac{\psi}{2} - \ln\left|\tan \frac{\psi}{4}\right| + B \tag{A.16}$$

where ψ is the running slope angle and B is an integration constant. The latter is determined by the boundary

(27) Derjaguin, B. V. *Dokl. Akad. Nauk USSR* **1946**, *51*, 517.
(28) Princen, H. M. In *Surface and Collod Science*; Matijević, E., Eirich, F. R., Eds.; Wiley: New York, 1969; Vol. 2, p 1.

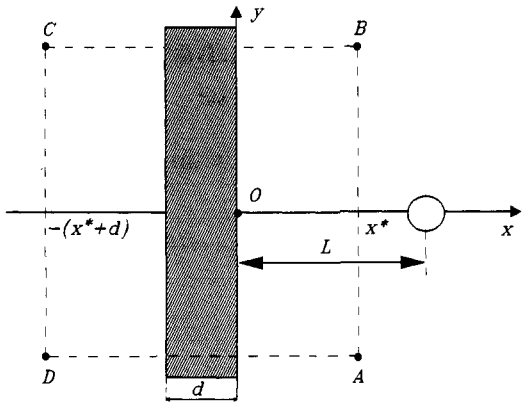

Figure 11. Integration contour for calculating the force between a capillary and a plate.

condition at the wall surface ($\psi|_{x=0} \equiv \psi_2$)

$$B = 2\cos\left(\frac{\psi_2}{2}\right) + \ln\left|\tan\left(\frac{\psi_2}{4}\right)\right| \qquad (A.17)$$

Equation A.17 can be expressed also in terms of the three-phase contact angle α_2; see eq 2.3.

Far away from the wall $\sin^2\psi \ll 1$ and the combination of eqs A.15 and A.16 predicts an exponential decay of the surface deformation

$$z(x) = \frac{1}{q}D\exp(-qx) \qquad (A.18)$$

$$\sin^2\psi(x) \ll 1$$

where

$$D = 4\exp(B-2) \qquad (A.19)$$

If the contact angle α_2 is close to $\pi/2$ ($\psi_2 \ll 1$) one obtains

$$z(x) = \frac{\cot\alpha_2}{q}e^{-qx} \qquad (A.20)$$

which is just the solution of the linearized Laplace equation.

Let us consider now the capillary interaction between a vertical cylinder and a wall; see Figures 1b and 11. If the separation between the two bodies is large enough ($qL > 2$), the slope of the meniscus in a certain intermediate zone between them will be small. Then one can apply the nonlinear superposition approximation. It is convenient to choose the contour of integration as shown in Figure 11. The square ABCD in Figure 11 is situated symmetrically with respect to the solid plate of thickness d. The side AB lays entirely in the region where the meniscus slope is small. The integrals of the forces acting on the sides BC and DA cancel each other. The forces on the other two sides can be calculated if we assume that the meniscus elevation at CD is given by eq A.18, i.e.

$$\zeta[x = -(x^* + d)] = \frac{1}{q}D\exp(-qx^*) \qquad (A.21)$$

and along the side AB, ζ is a superposition of the deformations created by the wall and the cylinder (see eq A.9)

$$\zeta(x = x^*) = \frac{1}{q}D\exp(-qx^*) + Q_1K_0(q((L-x^*)^2 + y^2)^{1/2}) \qquad (A.22)$$

For the force due to the interfacial tension, one can derive (see also eq A.4)

$$F^{(\gamma)} = \mathbf{e}_x\cdot\int_L\gamma\,\mathrm{d}l \approx \gamma\int_0^\infty\left[\left(\frac{\partial\zeta}{\partial y}\right)^2_{x=x^*} - \left(\frac{\partial\zeta}{\partial x}\right)^2_{x=x^*} + \left(\frac{\partial\zeta}{\partial x}\right)^2_{x=-x^*-d}\right]\mathrm{d}y \qquad (A.23)$$

For the force due to the hydrostatic pressure one obtains (see eqs A.5 and A.6)

$$F^{(p)} = \Delta\rho g\int_0^\infty[\zeta^2(x=x^*) - \zeta^2(x=-x^*-d)]\,\mathrm{d}y \qquad (A.24)$$

The combination of eqs A.8 and A.21–A.24 leads to the following expression for the capillary force

$$F = 2\pi\gamma DQ_1e^{-qL} + I \qquad (A.25)$$

where I denotes the integral

$$I = \gamma q^2Q_1^2\int_0^\infty\left[K_1^2(q(l^{*2}+y^2)^{1/2})\frac{y^2-l^{*2}}{l^{*2}+y^2} + K_0^2(q(l^{*2}+y^2)^{1/2})\right]\mathrm{d}y \qquad (A.26)$$

Here $l^* = L - x^*$

At large values of the argument the modified Bessel functions have identical asymptotes

$$K_n(t) = \left(\frac{\pi}{2t}\right)^{1/2}e^{-t}\left[1 + O\left(\frac{1}{t}\right)\right]$$

$$n = 0, 1, \ldots; \qquad t \gg 1$$

Then one can transform the integral I to read

$$I \approx \pi\gamma qQ_1^2\int_0^\infty\frac{y^2}{(l^{*2}+y^2)^{3/2}}\exp(-2q(l^{*2}+y^2)^{1/2})\,\mathrm{d}y \qquad (A.27)$$

$$ql^* > 1$$

The integrand in eq A.27 is smaller than $\exp(-2ql^*)$. Hence

$$I < \frac{1}{2}\pi\gamma qQ_1^2e^{-2ql^*} \qquad (A.28)$$

Since $2l^* \approx L$ one can evaluate (see eq A.25)

$$F = 2\pi\gamma Q_1De^{-qL}\left[1 + O\left(\frac{qQ_1}{4D}\right)\right] \qquad (A.29)$$

The second term in the right hand side of eq A.29 can be neglected if ψ_2 is not very close to zero. Indeed, $D \approx \tan\psi_2$ at small values of ψ_2 (see eq 2.9). Therefore the second term in the above equation is negligible if $qQ < \tan\psi_2$ (please note that in the case under consideration $qQ \ll 1$). Thus eq A.29 reduces to eq 2.8 which is the asymptotic expression for the interaction force between the wall and the capillary. The final result does not depend on the exact choice of the contour of integration (x^* and l^* are absent in eq A.29) as should be expected.

The integration of eqs A.14 and A.29 with respect to the interparticle distance L gives the corresponding energy of capillary interaction.